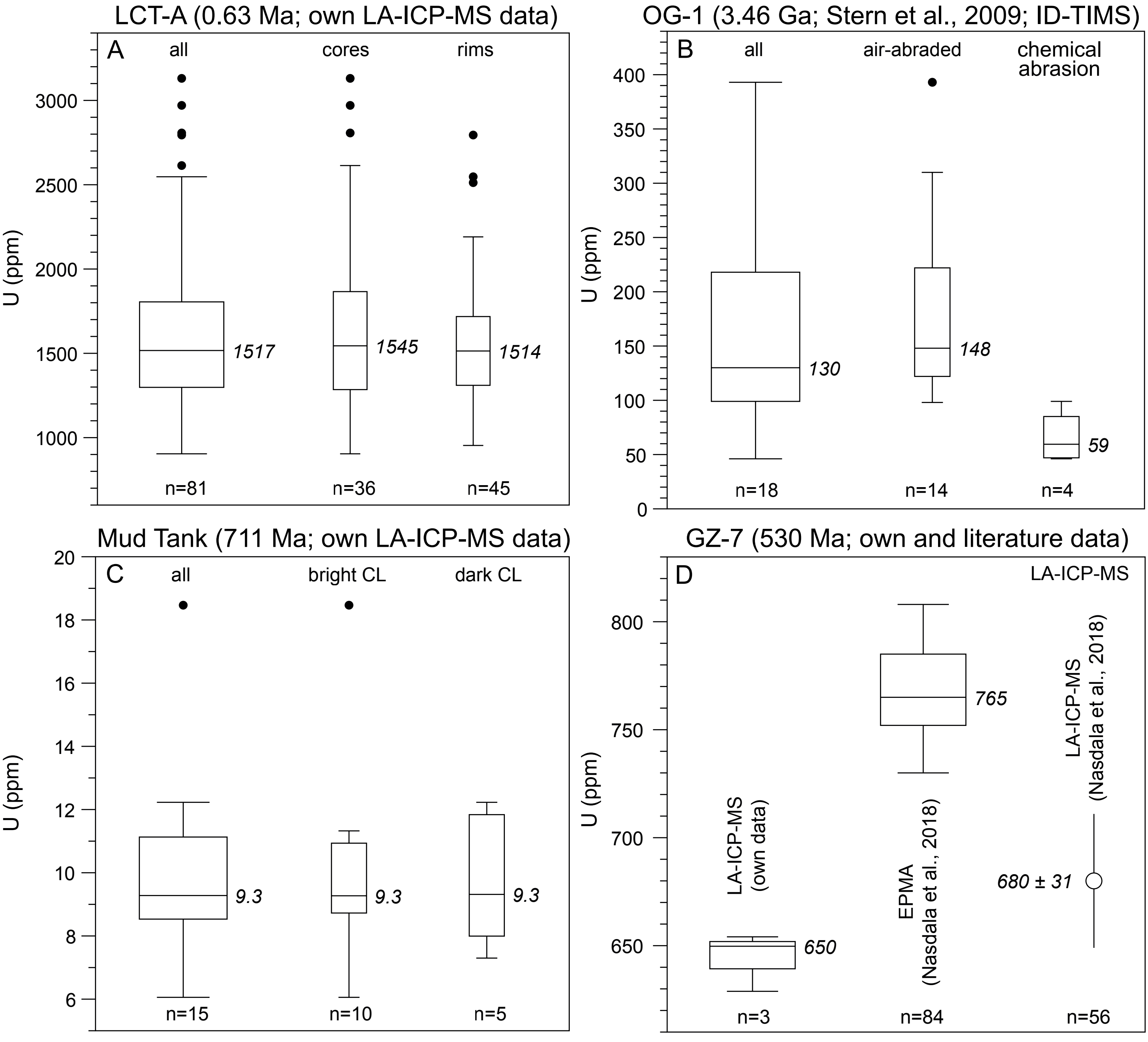


Figure S1: U concentration (ppm) of test zircon used in this study. LCT-A-Lava Creek Tuff Unit A zircon, OG-1-Owens Gully Diorite zircon.

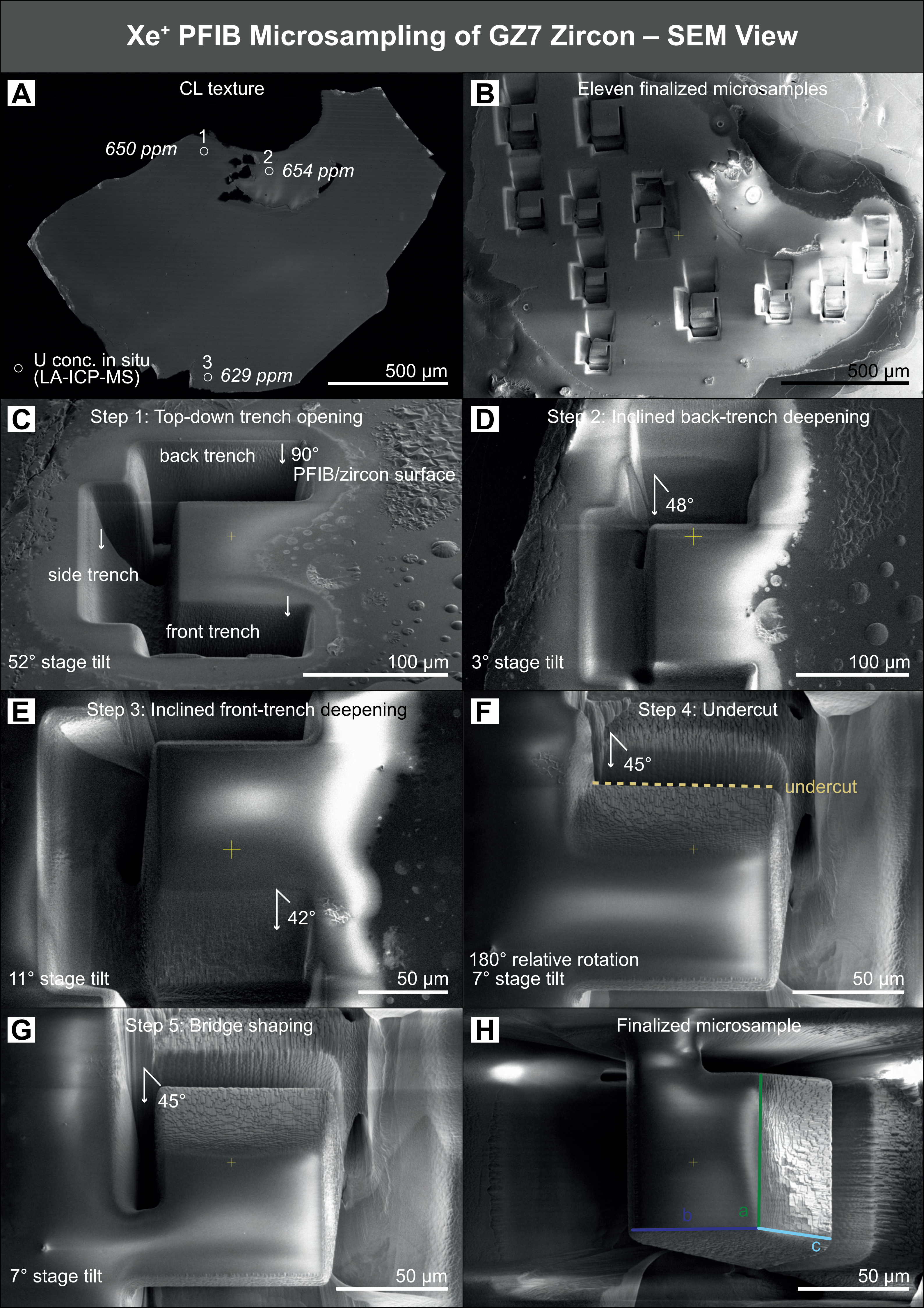


Figure S2: (A) Cathodoluminescence (CL) texture and in situ U concentration of the microsampled GZ7 zircon reference material. (B) Eleven microsamples of GZ7 zircon machined using $Xe^{+}$ PFIB. (C–H) Scanning electron microscope view of the step-by-step microsampling procedure. Angles next to arrows refer to angles of the PFIB objective with respect to zircon surface at different machining steps. (H) Sides labelled a, b and c correspond to those in Figure 6B and C in the main text.

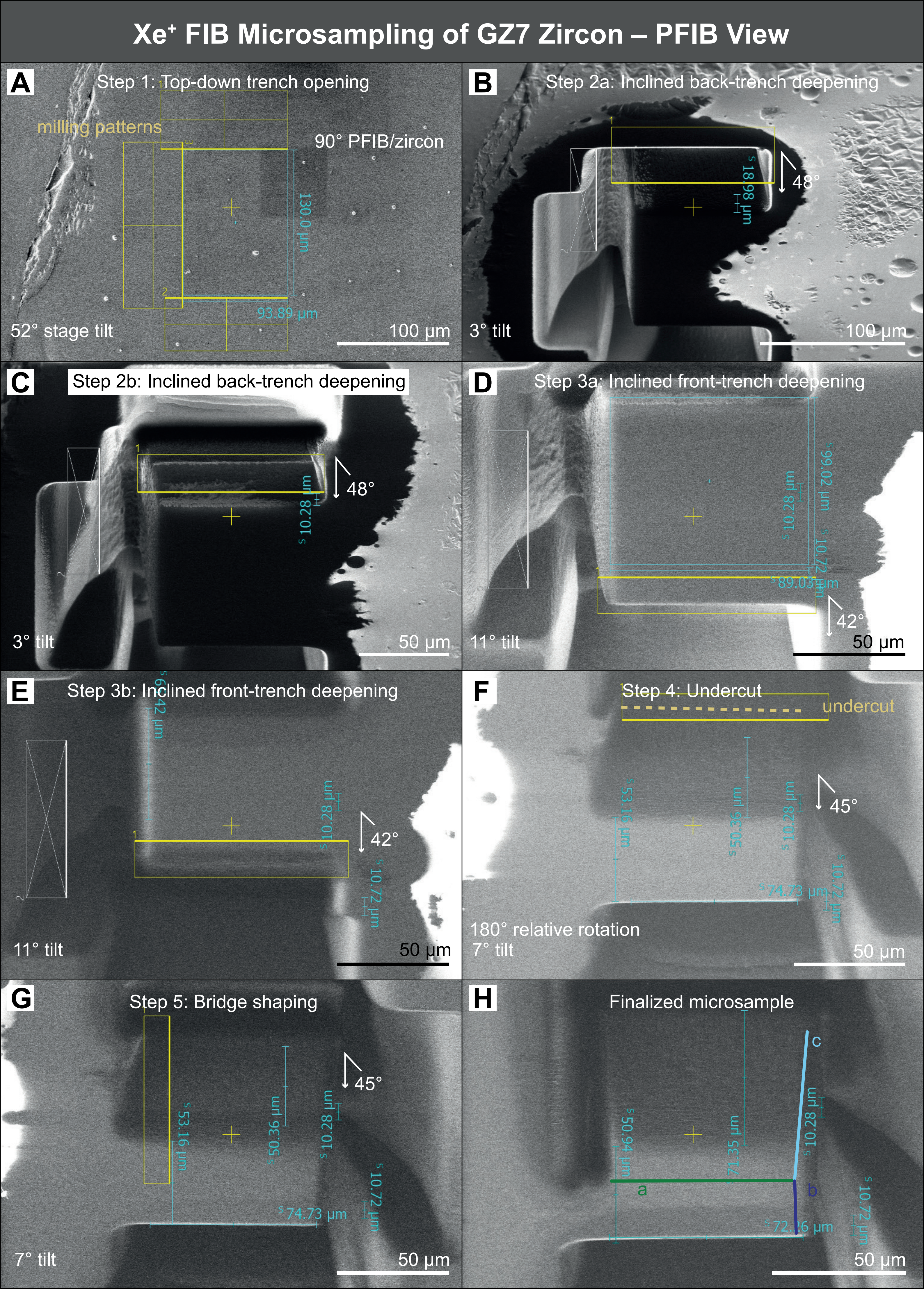


Figure S3: (A–H) Plasma focused ion beam (PFIB) view of the step-by-step zircon microsampling. Yellow rectangles represent PFIB machining patterns. Angles next to arrows refer to angles of the PFIB objective with respect to zircon surface at different machining steps. (H) Sides labelled a, b and c correspond to those in Figure 6B and C in the main text.

# Femtosecond Laser Microsampling of GZ7 Zircon – SEM View

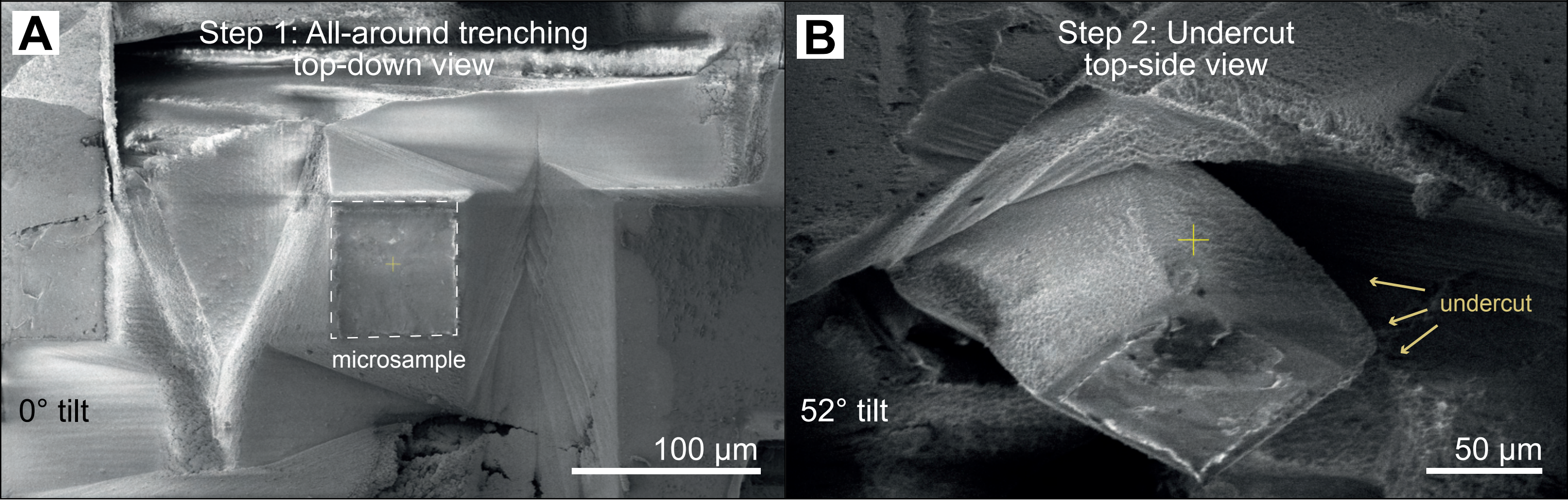


Figure S4: (A) Initial trench opening and (B) undercut during femtosecond laser zircon microsampling.

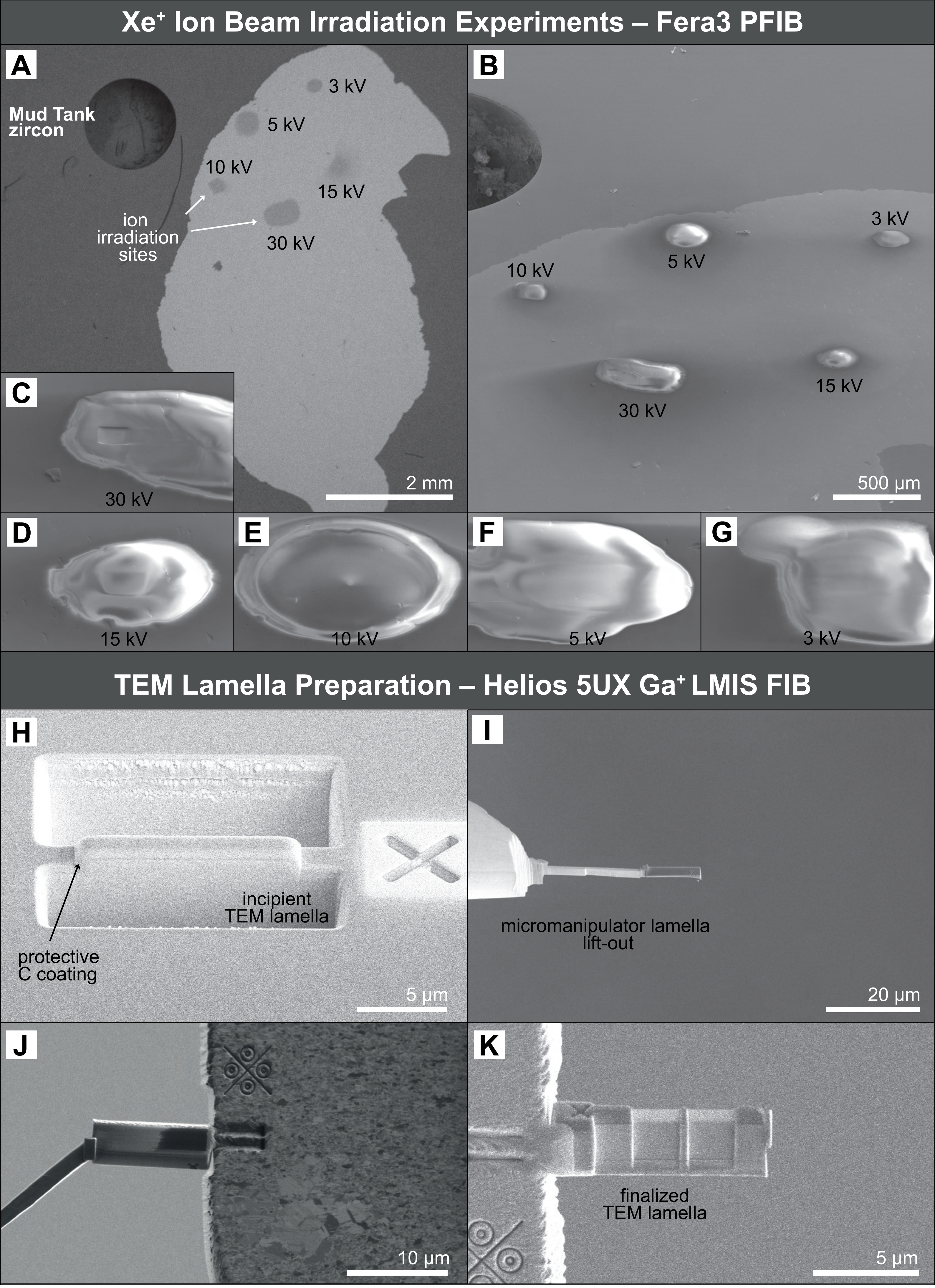


Figure S5: (A–G) $Xe^+$ irradiation experiments at different voltages (30–3 kV) on Fera3 PFIB and (H–K) preparation of TEM lamellae from the irradiated sites. LMIS-liquid metal ion source.

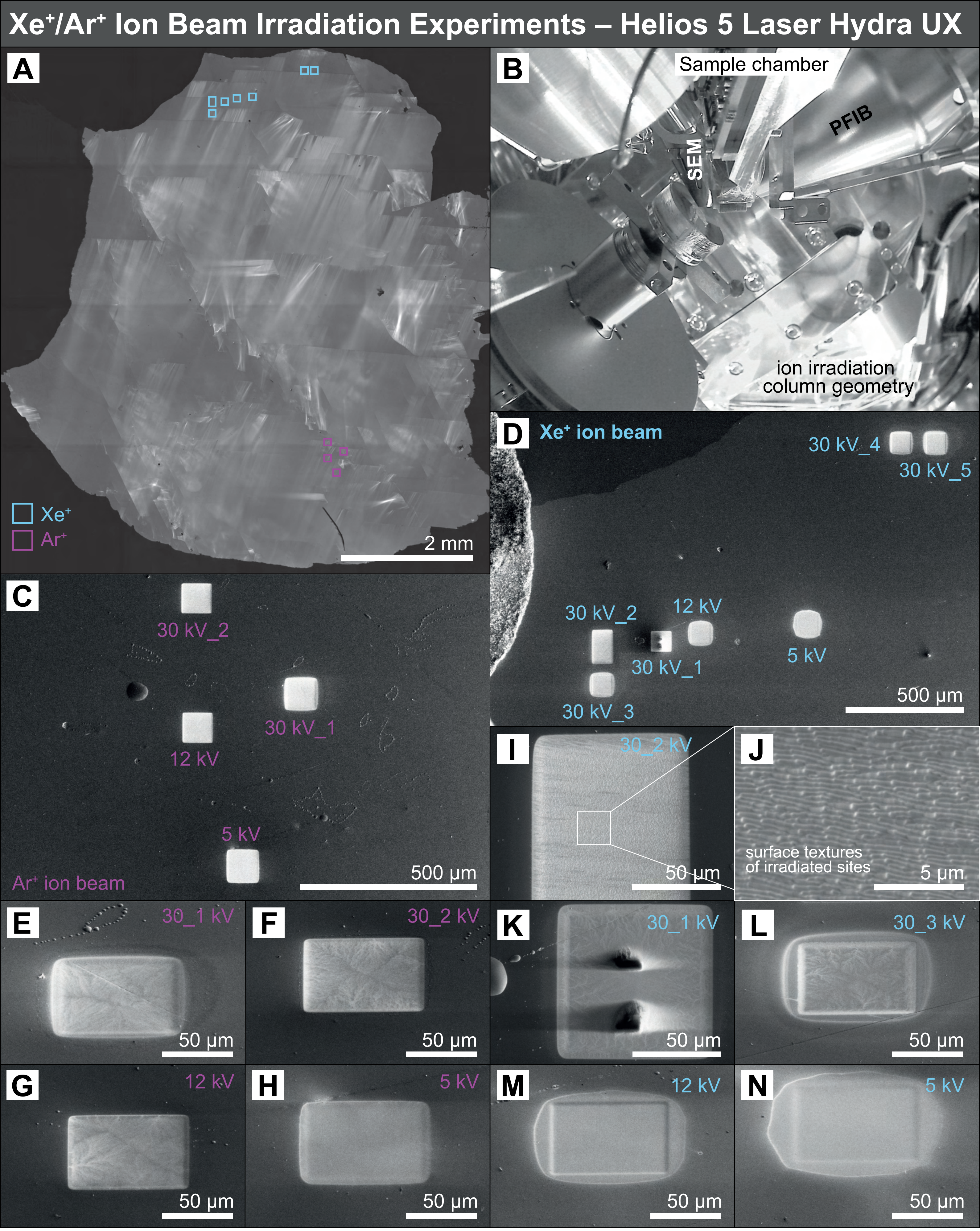


Figure S6: $Xe^{+}/Ar^{+}$ irradiation experiments at different voltages (30–5 kV) on Hydra PFIB.
(A) Cathodoluminescence texture of the Mud Tank zircon used for the irradiation experiments. (B) PFIB column geometry during ion machining. (C–N) Sites on Mud Tank zircon irradiated at different ion beam voltages.

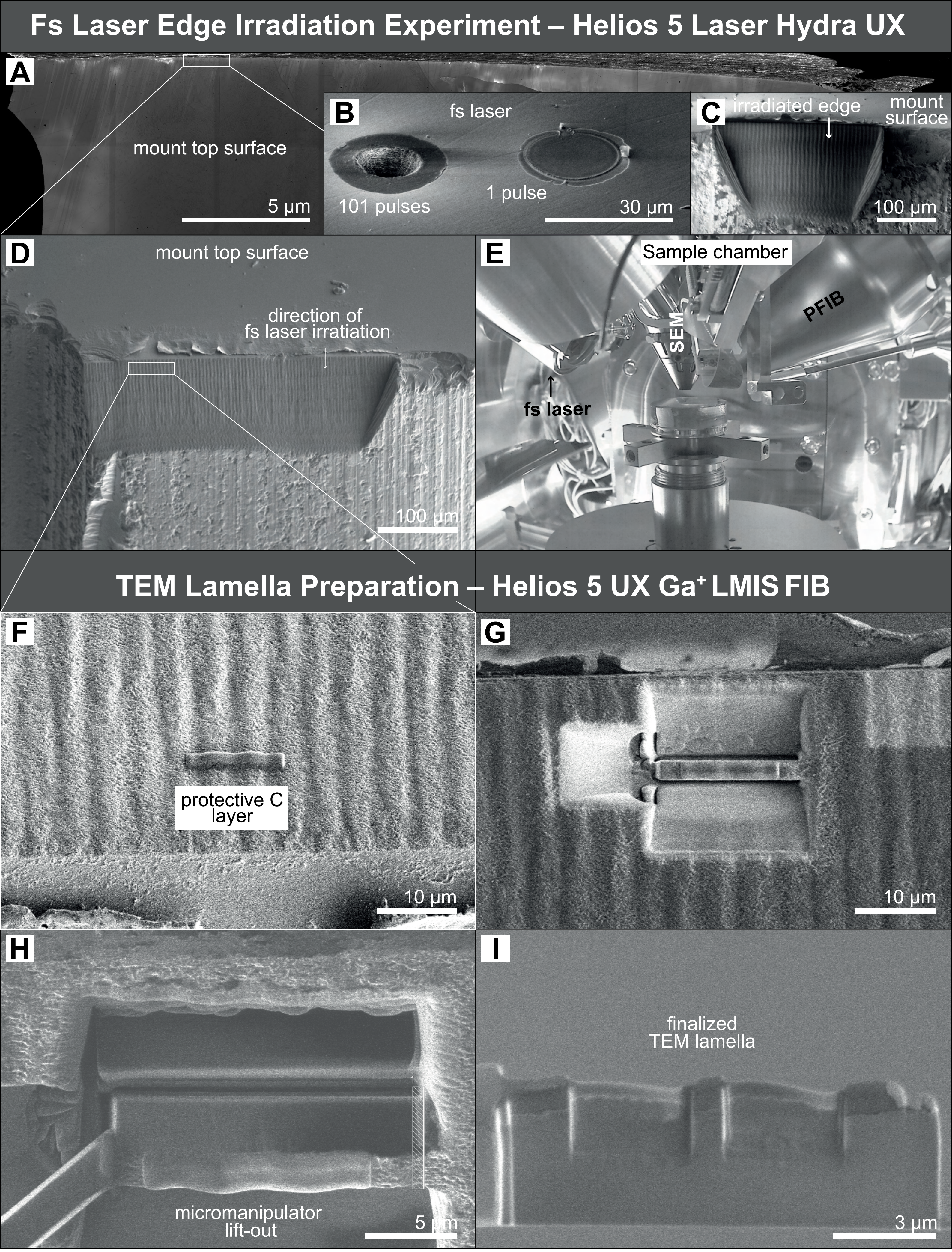


Figure S7: Femtosecond laser (515 nm wavelength) irradiation experiment on an exposed edge of a Mud Tank zircon. (A) Cathodoluminescence (CL) texture of the irradiated Mud Tank zircon. (B) Surface halo and lack of debris after femtosecond laser machining. (C and D) Curtained surface topography of a laser crater wall. (E) View of the sample chamber showing the main elements. For normal incidence laser irradiation, a pre-tilted holder (60 °) is used to orient the zircon surface at a 90 ° angle with respect to the laser objective (not shown). (F–I) Selected steps of the preparation of a TEM lamella from the irradiated edge. LMIS-liquid metal ion source.

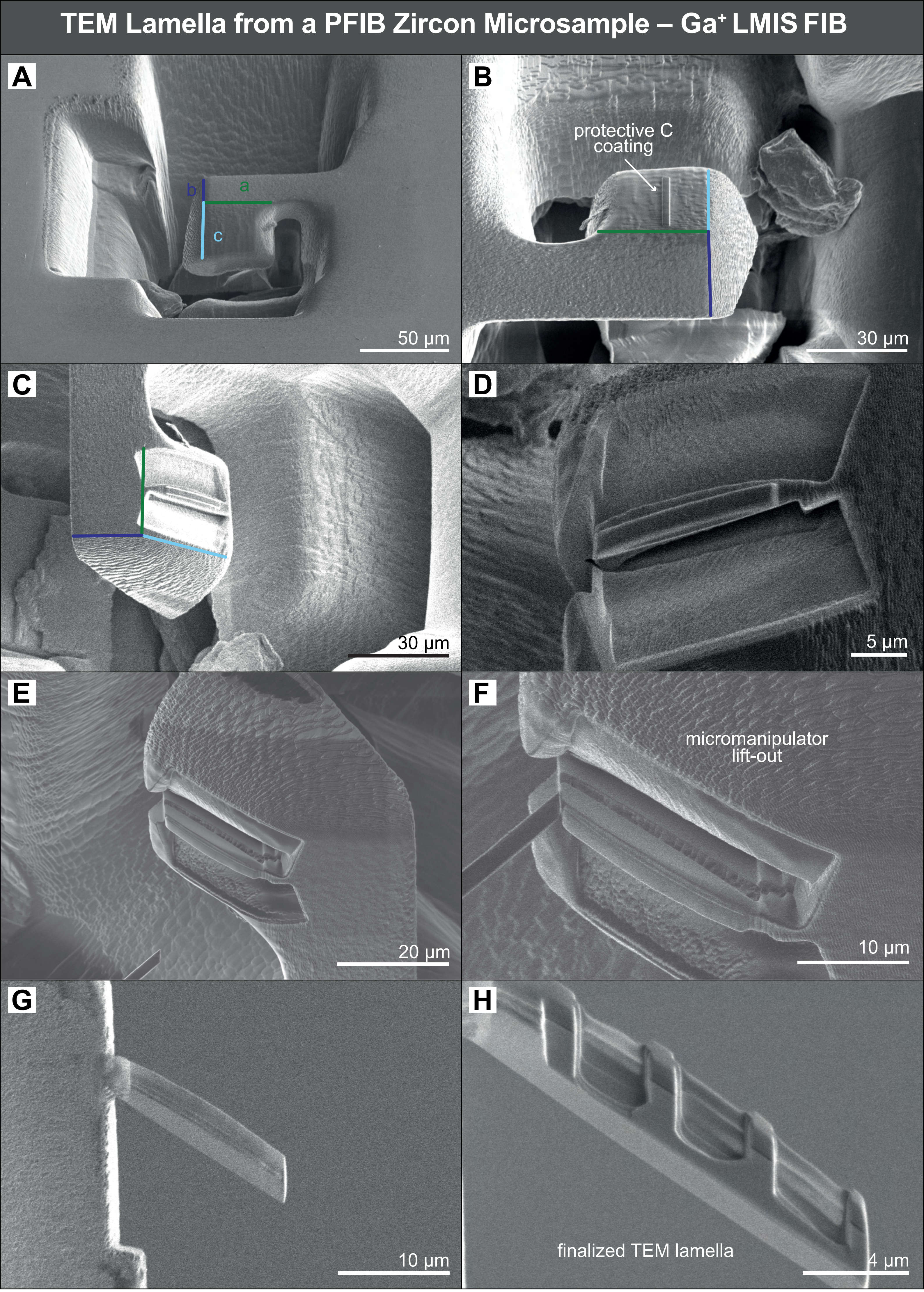


Figure S8: TEM lamella preparation from a Xe⁺ PFIB-machined Mud Tank microsample. Marked microsample edges in A–C correlate with those in Figure 6B and C in the main text. LMIS-liquid metal ion source.

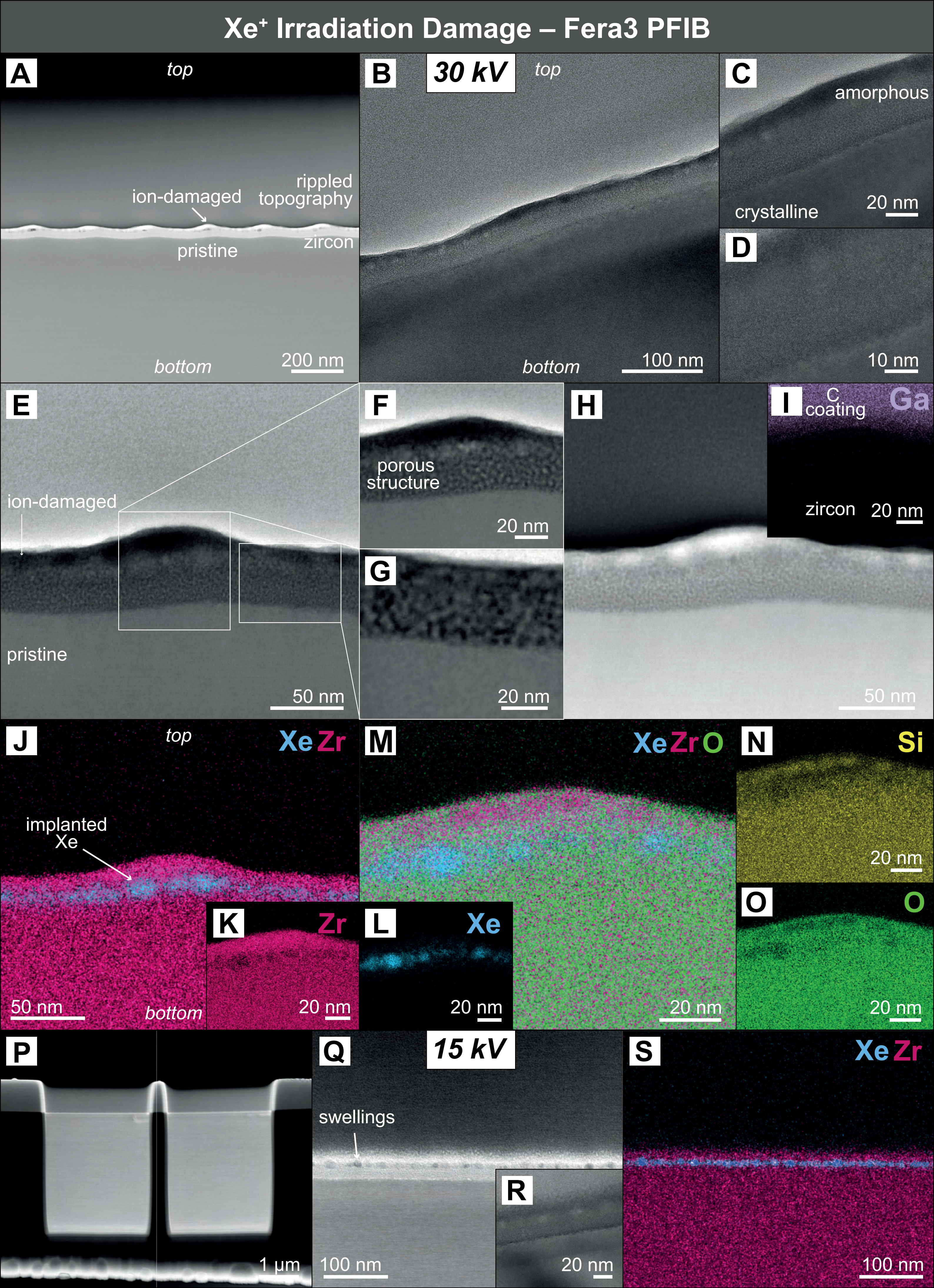
Xe+ Irradiation Damage – Fera3 PFIB
A
top
ion-damaged
rippled topography
pristine
zircon
bottom
200 nm
B
30 kV
top
bottom
100 nm
C
amorphous
crystalline
20 nm
D
10 nm
E
ion-damaged
pristine
50 nm
F
porous structure
20 nm
G
20 nm
H
50 nm
I
C coating
Ga
zircon
20 nm
J
top
Xe Zr
implanted Xe
50 nm
bottom
K
Zr
20 nm
L
Xe
20 nm
M
Xe Zr O
20 nm
N
Si
20 nm
O
O
20 nm
P
1 µm
Q
15 kV
swellings
100 nm
R
20 nm
S
Xe Zr
100 nm

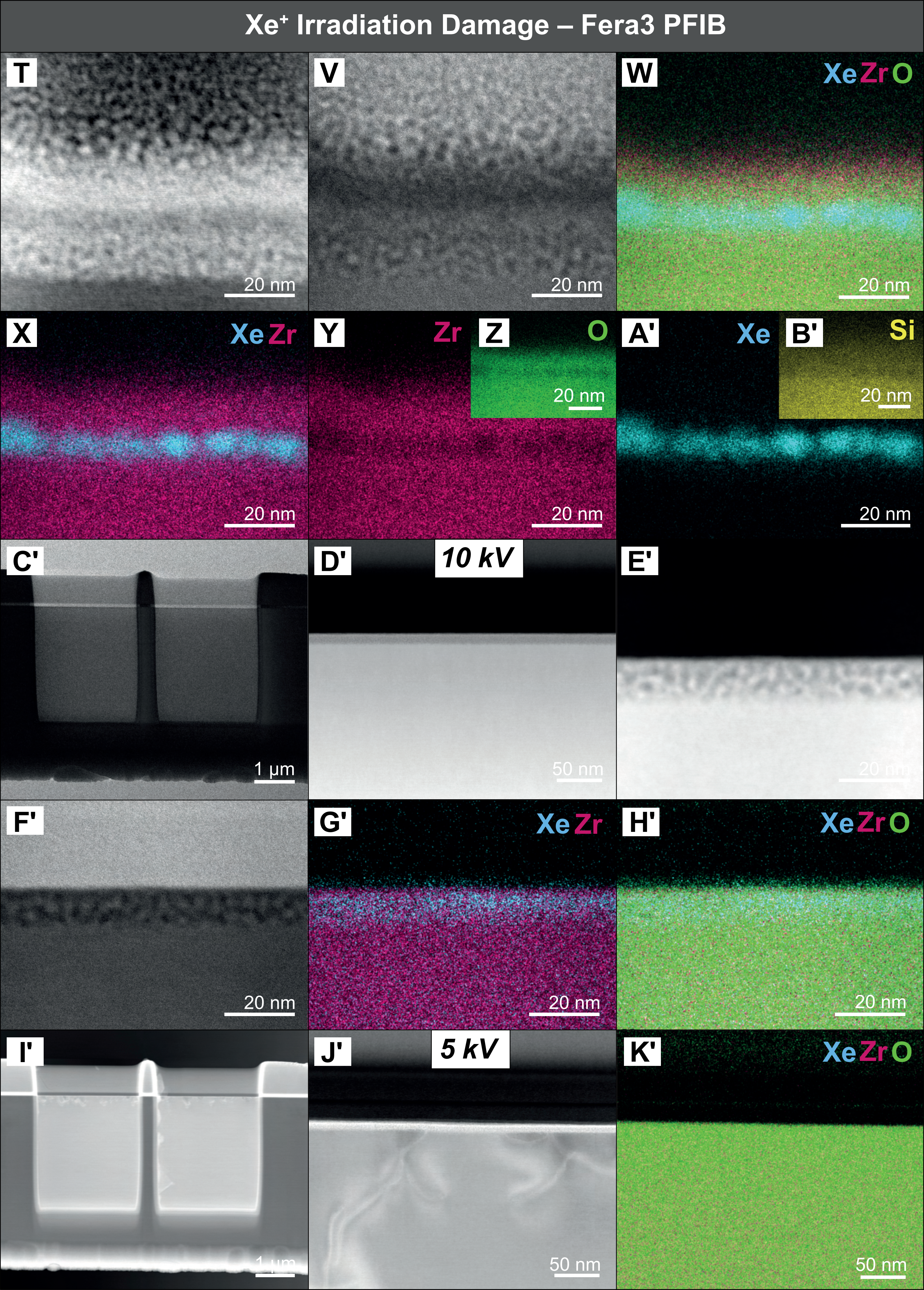
Xe+ Irradiation Damage – Fera3 PFIB
T
20 nm
V
20 nm
W
Xe Zr O
20 nm
X
Xe Zr
20 nm
Y
Zr
Z
O
20 nm
20 nm
A'
Xe
B'
Si
20 nm
20 nm
C'
1 µm
D'
10 kV
50 nm
E'
F'
20 nm
G'
Xe Zr
20 nm
H'
Xe Zr O
20 nm
I'
J'
5 kV
50 nm
K'
Xe Zr O
50 nm

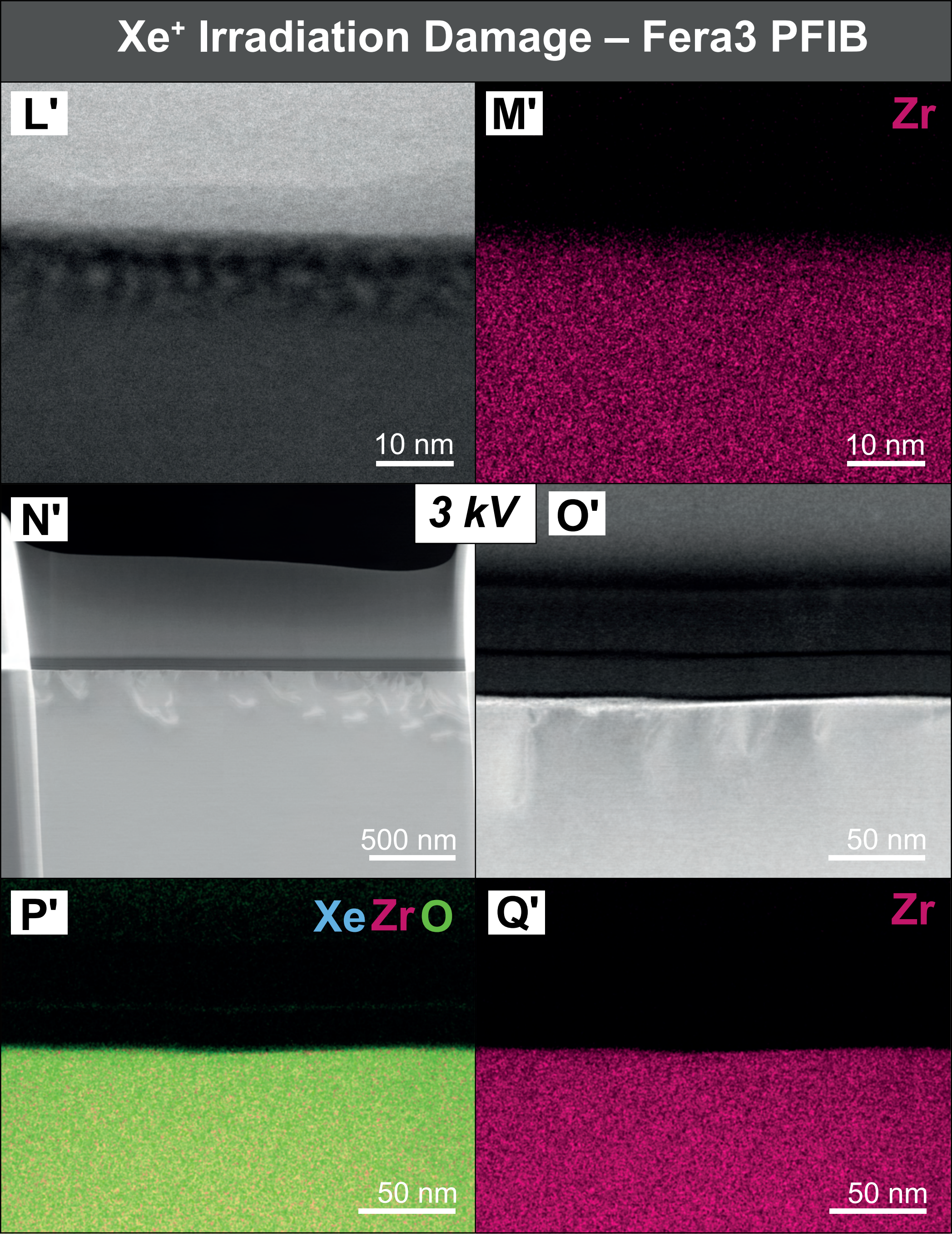


Figure S9: TEM images and EDS element maps of zircon damaged by $Xe^{+}$ irradiation at different voltages (30–3 kV) on Fera3 PFIB. The damaged zone is nanometers-thick, porous and amorphous, and exhibits a rippled surface for high voltage (30 kV and 15 kV) conditions. Element maps show implantation of $Xe^{+}$ in continuous layers within the damaged zone and local mobility of Zr, Si and O. Ga element map (I) shows no implantation of $Ga^{+}$ ions into zircon during TEM lamella preparation.

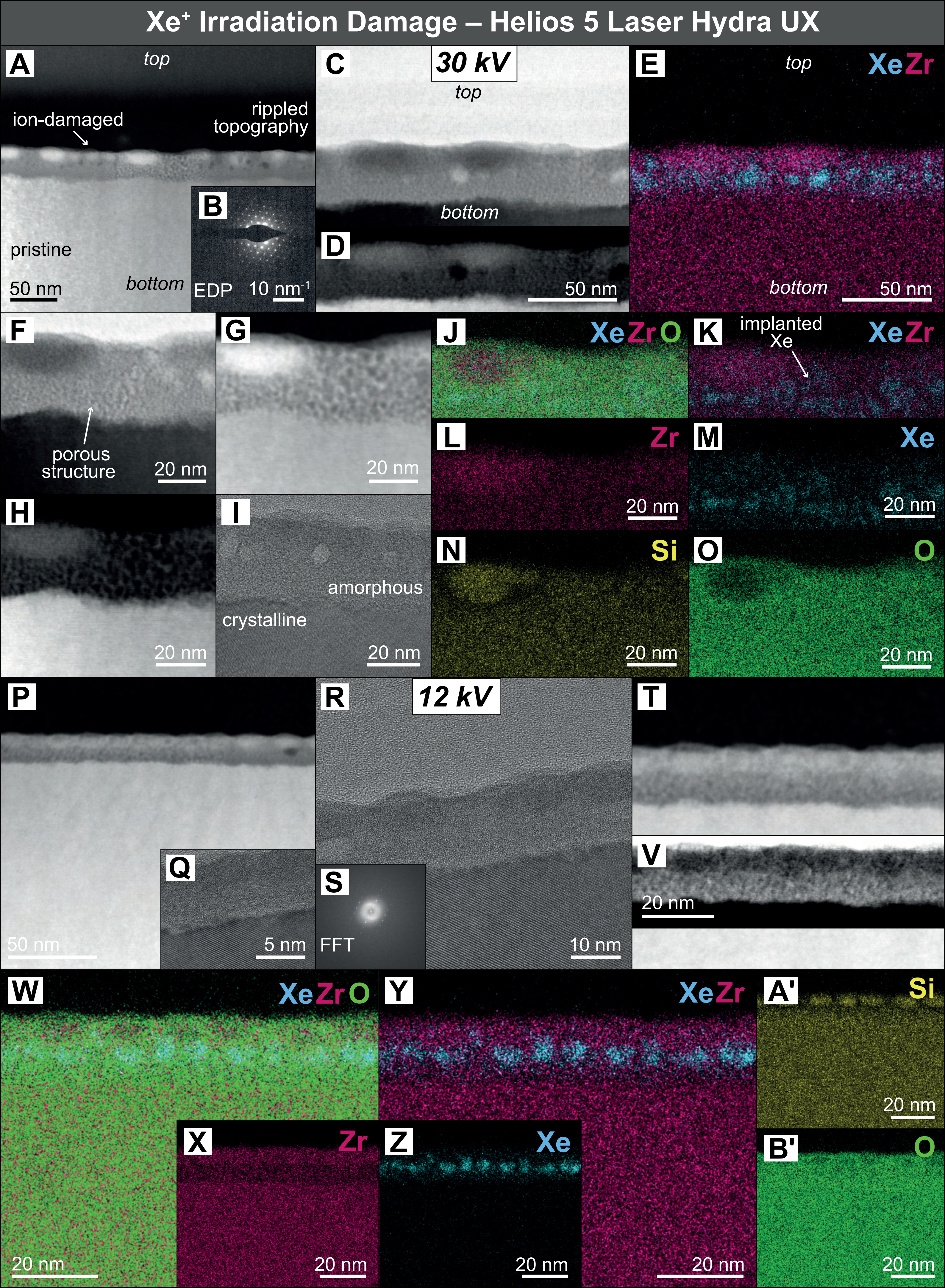

Xe+ Irradiation Damage – Helios 5 Laser Hydra UX
A
top
ion-damaged
rippled topography
pristine
bottom
50 nm
B
EDP
10 nm-1
C
30 kV
top
bottom
D
50 nm
E
top
XeZr
bottom
50 nm
F
porous structure
20 nm
G
20 nm
H
20 nm
I
amorphous
crystalline
20 nm
J
XeZrO
K
implanted Xe
XeZr
L
Zr
20 nm
M
Xe
20 nm
N
Si
20 nm
O
O
20 nm
P
50 nm
Q
5 nm
R
12 kV
S
FFT
10 nm
T
V
20 nm
W
XeZrO
20 nm
X
Zr
20 nm
Y
XeZr
20 nm
Z
Xe
20 nm
A'
Si
20 nm
B'
O
20 nm

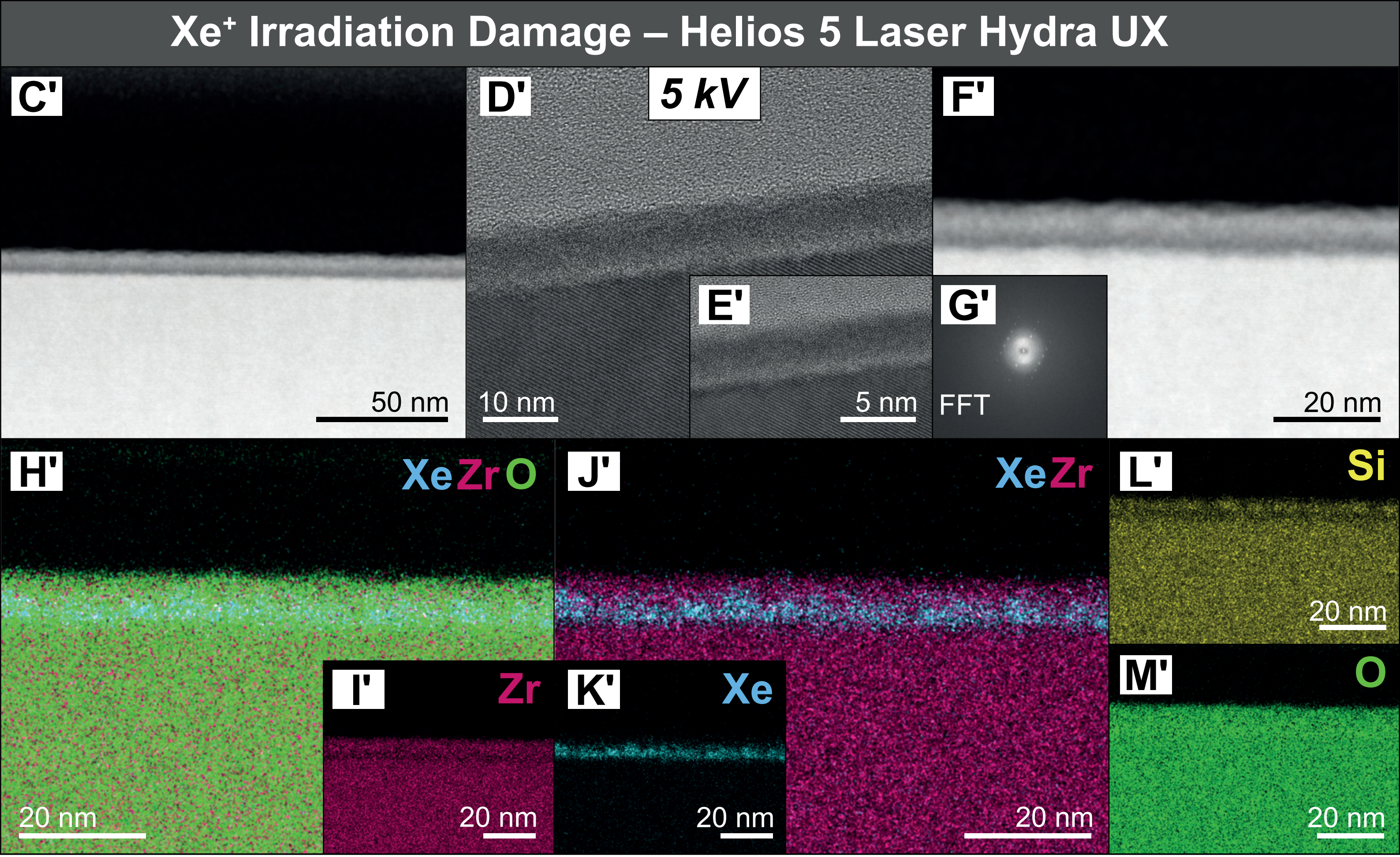


Figure S10: TEM images and EDS element maps of zircon damaged by $Xe^{+}$ irradiation at different voltages (30–5 kV) on Hydra PFIB. Electron diffraction (EDP) and fast Fourier transformation (FFT) patterns show a dominantly crystalline state of the analyzed TEM lamella from the irradiated zircon.

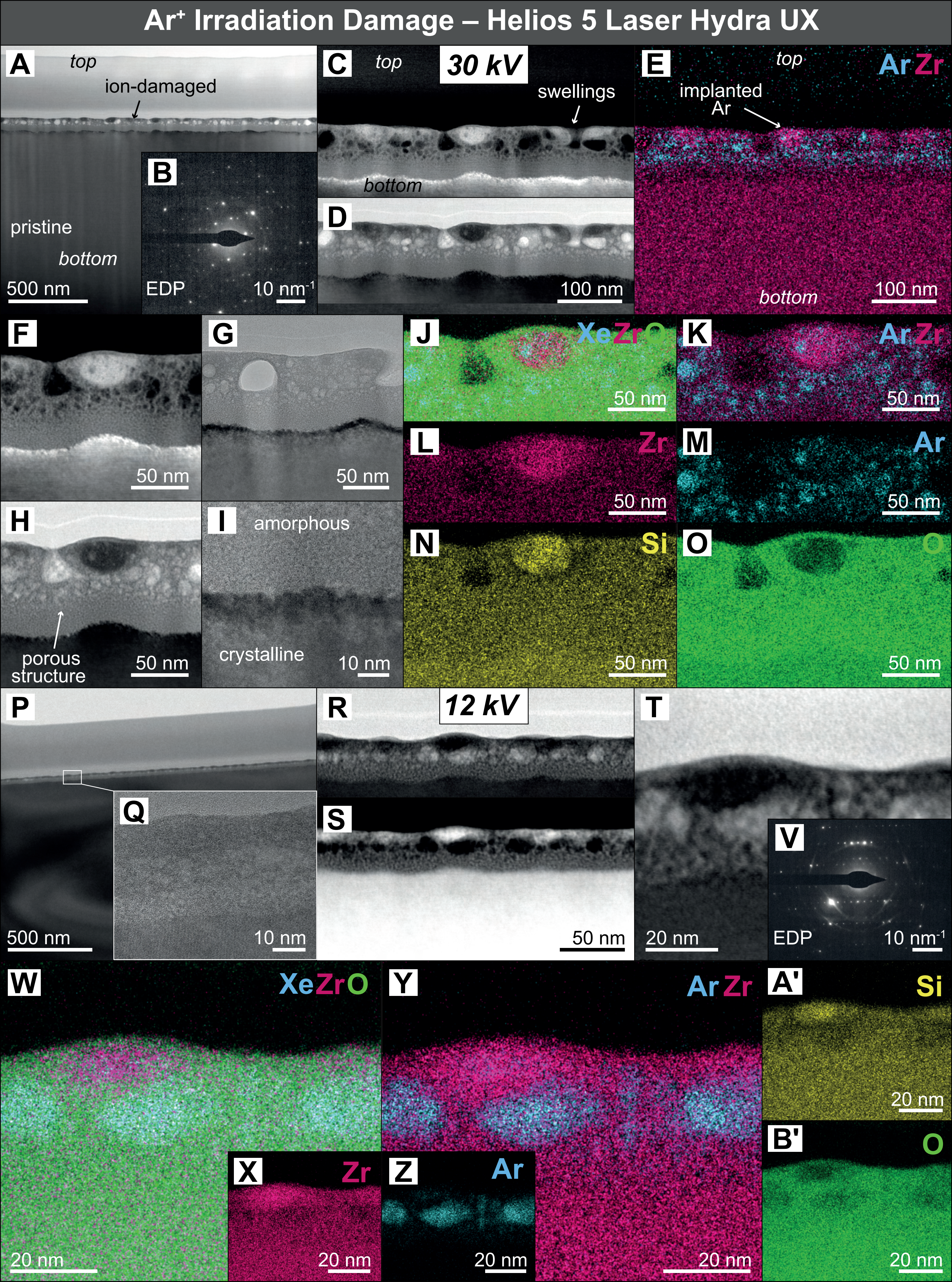

Ar+ Irradiation Damage – Helios 5 Laser Hydra UX
A
top
ion-damaged
pristine
bottom
500 nm
B
EDP
10 nm-1
C
top
30 kV
swellings
bottom
D
100 nm
E
top
Ar Zr
implanted Ar
bottom
100 nm
F
50 nm
G
50 nm
J
XeZrO
50 nm
K
Ar Zr
50 nm
L
Zr
50 nm
M
Ar
50 nm
H
porous structure
50 nm
I
amorphous
crystalline
10 nm
N
Si
50 nm
O
O
50 nm
P
500 nm
Q
10 nm
R
12 kV
S
50 nm
T
20 nm
V
EDP
10 nm-1
W
XeZrO
20 nm
Y
Ar Zr
20 nm
A'
Si
20 nm
X
Zr
20 nm
Z
Ar
20 nm
B'
O
20 nm

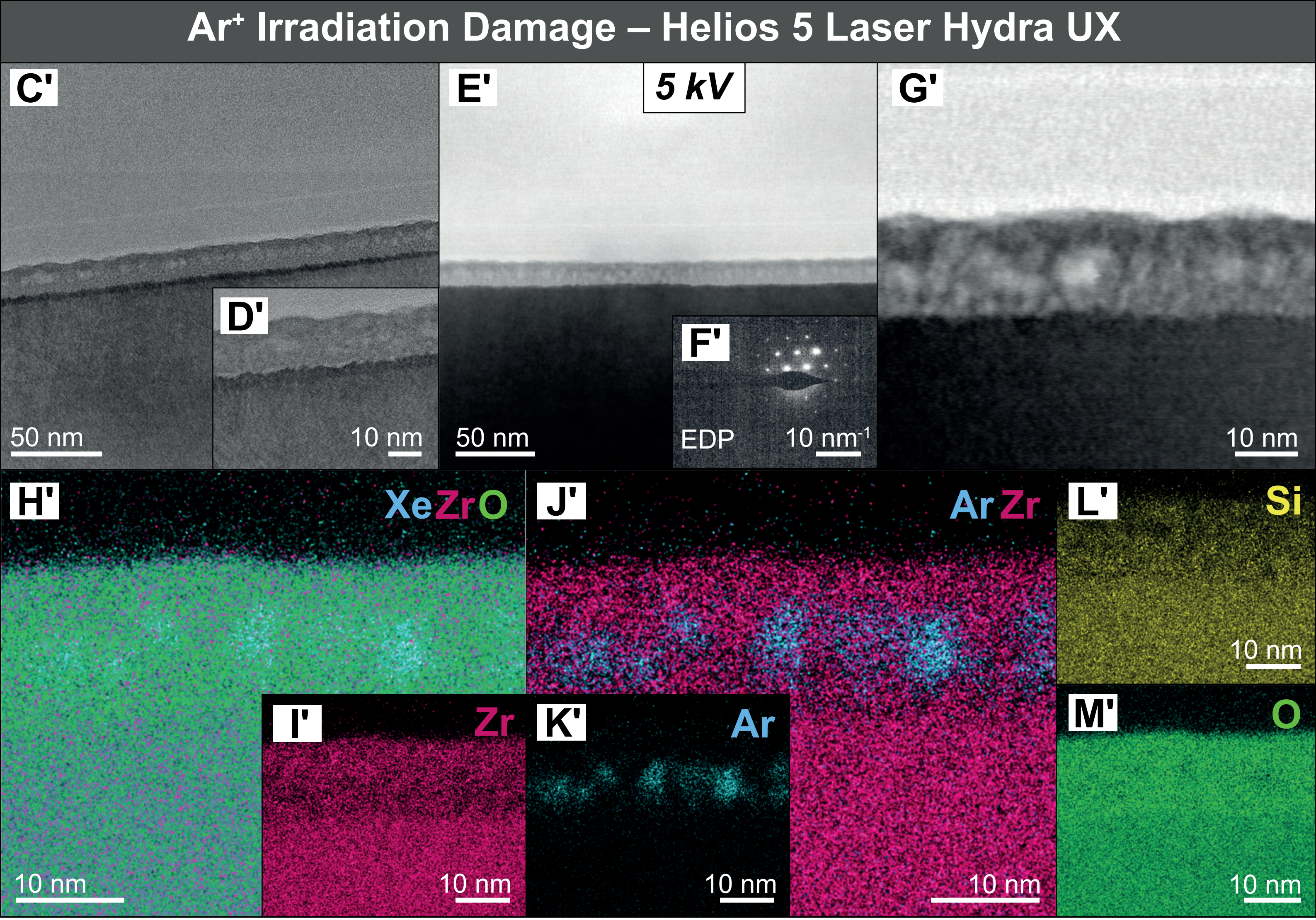


Figure S11: TEM images and EDS element maps of zircon damaged by $Ar^+$ irradiation at different voltages (30–5 kV) on Hydra PFIB. Electron diffraction (EDP) patterns show a dominantly crystalline state of the analyzed TEM lamella from the irradiated zircon.

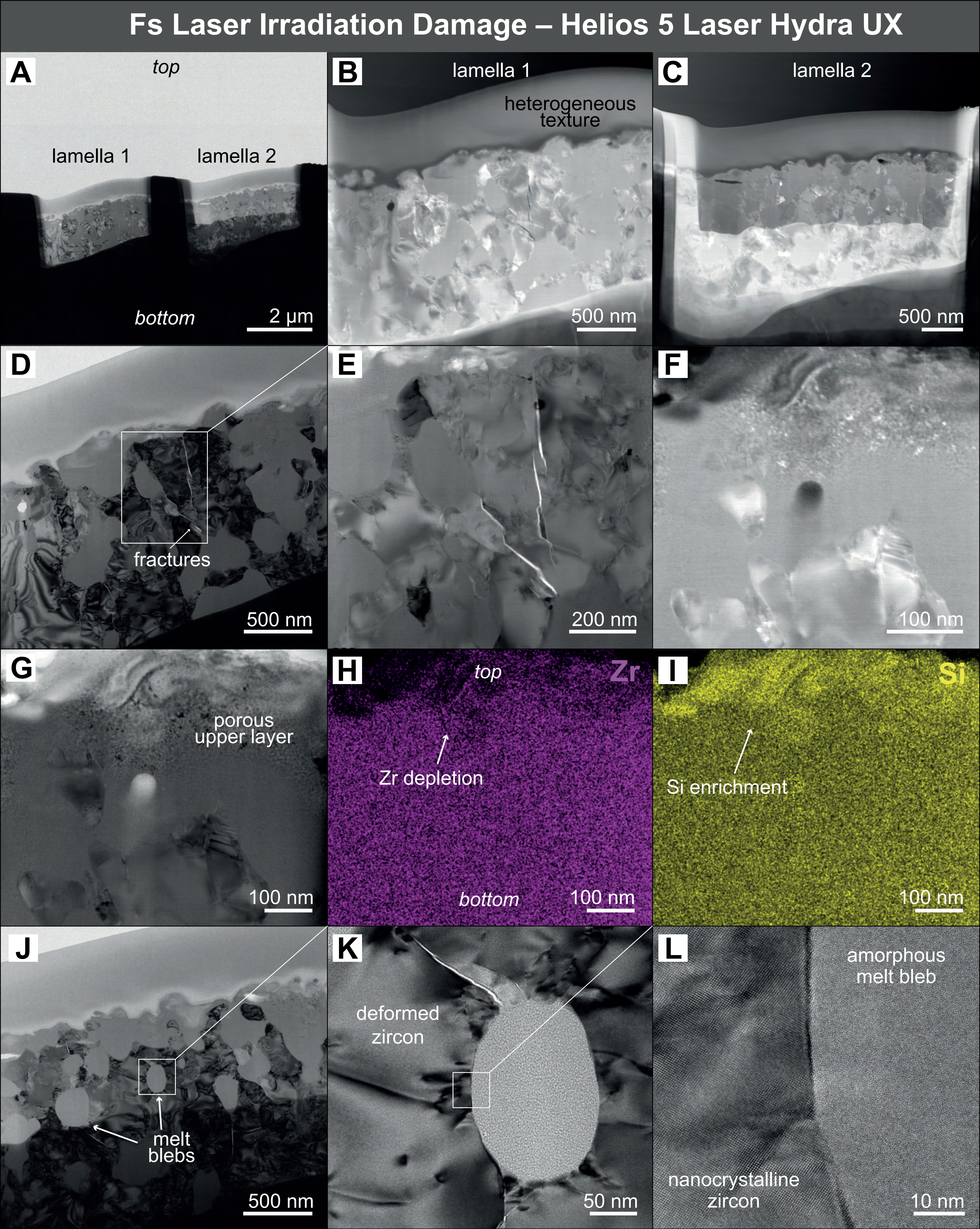
Fs Laser Irradiation Damage – Helios 5 Laser Hydra UX
A
top
lamella 1
lamella 2
bottom
2 µm
B
lamella 1
heterogeneous texture
500 nm
C
lamella 2
500 nm
D
fractures
500 nm
E
200 nm
F
100 nm
G
porous upper layer
100 nm
H
top
Zr
Zr depletion
bottom
100 nm
I
Si
Si enrichment
100 nm
J
melt blebs
500 nm
K
deformed zircon
50 nm
L
amorphous melt bleb
nanocrystalline zircon
10 nm

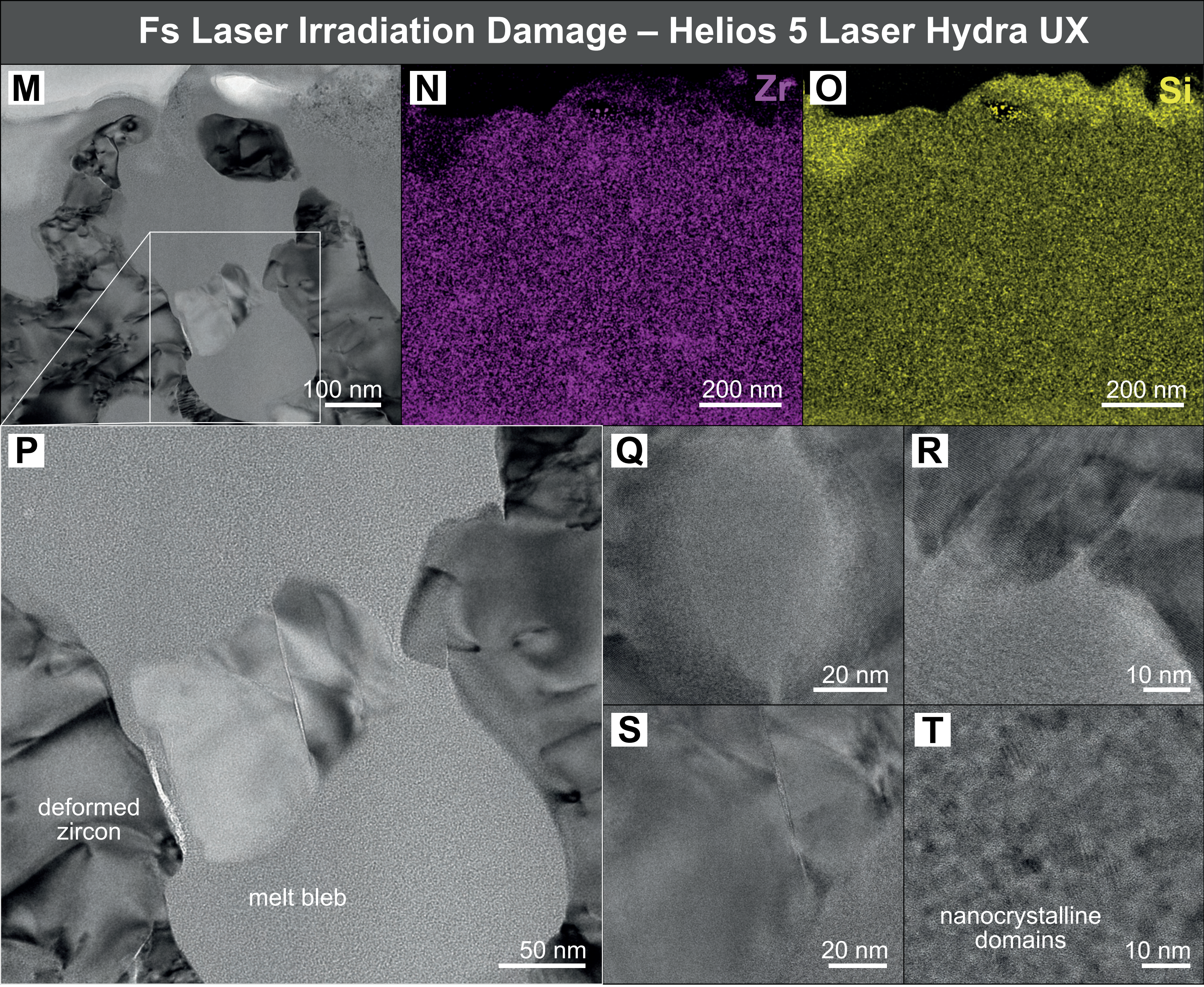


Figure S12: Damage in zircon induced by femtosecond laser machining (515 nm wavelength). TEM images and EDS element maps show a chaotic texture and mobility of Zr and Si in the topmost part immediately exposed to the laser beam. Whole TEM lamella (~2 µm) of laser-irradiated zircon is damaged and exhibits globular structures.

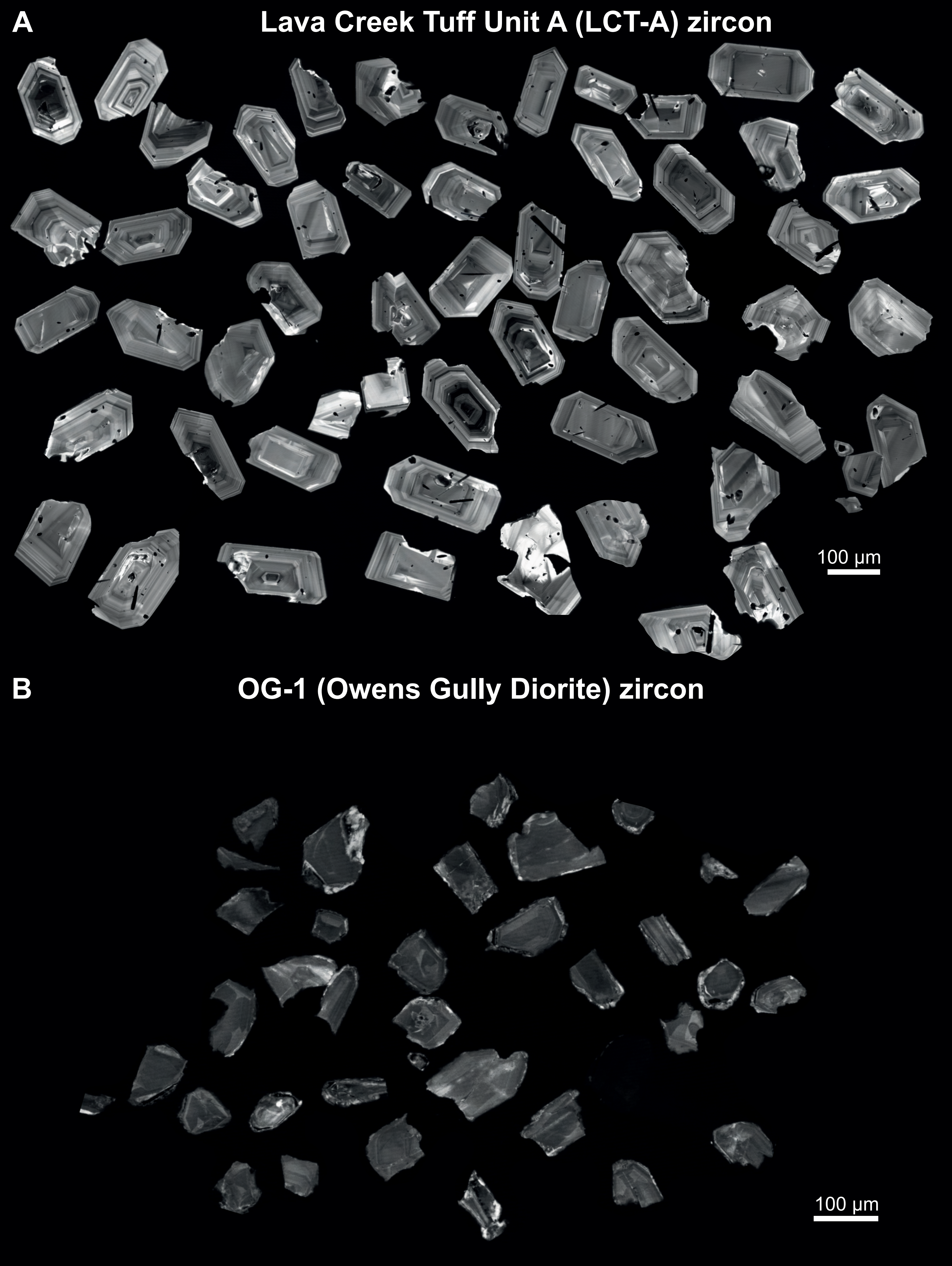


Figure S13: Cathodoluminescence (CL) texture of the Lava Creek Tuff Unit A (LCT-A) and Owen Gully Diorite (OG-1) zircon used in the experiments on the impact of coatings on U-Pb systematics.

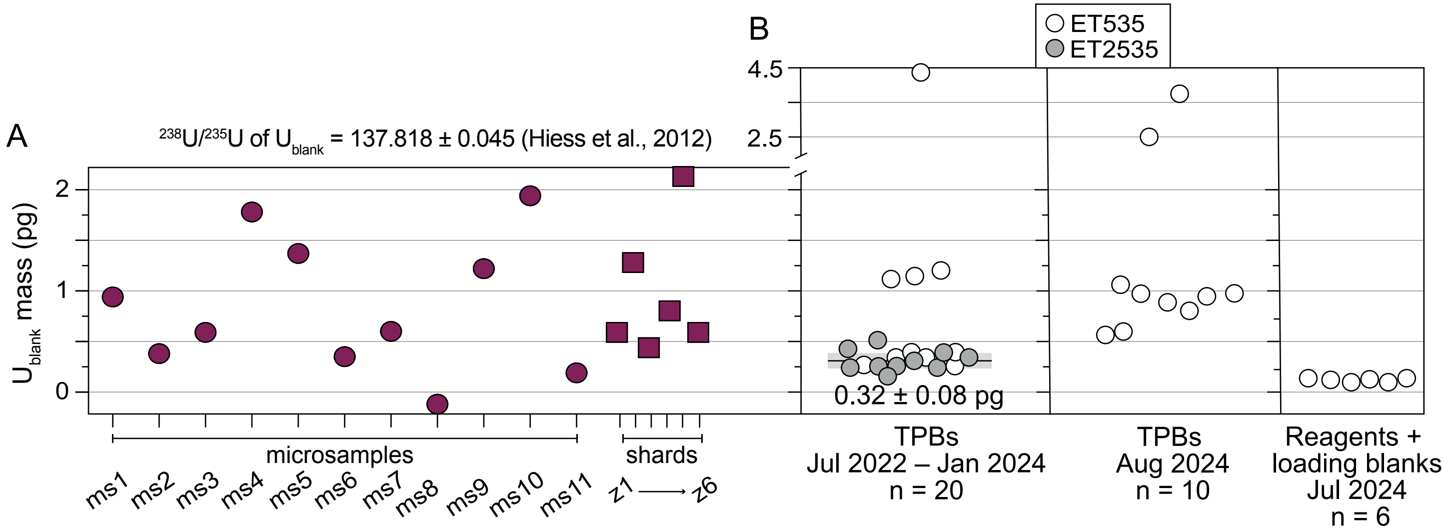


Fig. S14: (A) $U_{blank}$ mass correction for PFIB-machined Mud Tank microsamples and non-irradiated shards required to force concordance at 711 Ma (reference age given by large pieces). The correction assumes a $^{238}U/^{235}U$ of $U_{blank}$ of 137.8185 ± 0.045 of magmatic zircon (Hiess et al., 2012).
(B) Mass of U (pg) measured in total procedural blanks (TPBs) and in reagents blanks (including the loading blank) prepared with both ET535 and ET2535 tracer solutions. The reagent blanks were prepared from 30 drops of 6N HCl and 24 drops of $H_2O$ (representative of amounts used to elute Pb and U during chemistry), spiked with one drop of ET535 tracer solution, and dried down with one drop of $H_3PO_4$ acid in beakers used for samples.